

# Nanofiber Air Filters with High-Temperature Stability for Efficient PM<sub>2.5</sub> Removal from the Pollution Sources

Rufan Zhang,<sup>†</sup> Chong Liu,<sup>†</sup> Po-Chun Hsu,<sup>†</sup> Chaofan Zhang,<sup>§</sup> Nian Liu,<sup>†</sup> Jinsong Zhang,<sup>†</sup> Hye Ryoung Lee,<sup>†</sup> Yingying Lu,<sup>†</sup> Yongcai Qiu,<sup>†</sup> Steven Chu,<sup>‡</sup> and Yi Cui<sup>\*,†,§</sup>

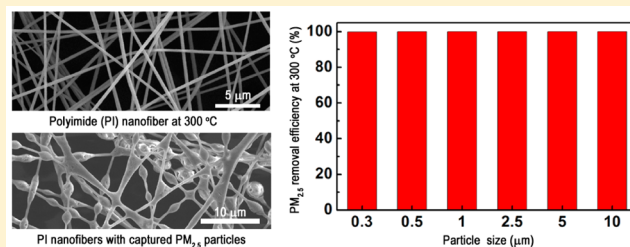
<sup>†</sup>Department of Materials Science and Engineering and <sup>‡</sup>Department of Physics, Stanford University, Stanford, California 94305, United States

<sup>§</sup>Stanford Institute for Materials and Energy Sciences, SLAC National Accelerator Laboratory, 2575 Sand Hill Road, Menlo Park, California 94025, United States

## S Supporting Information

**ABSTRACT:** Here, we developed high-efficiency (>99.5%) polyimide-nanofiber air filters for the high temperature PM<sub>2.5</sub> removal. The polyimide nanofibers exhibited high thermal stability, and the PM<sub>2.5</sub> removal efficiency was kept unchanged when temperature ranged from 25–370 °C. These filters had high air flux with very low pressure drop. They could continuously work for >120 h for PM<sub>2.5</sub> index >300. A field-test showed that they could effectively remove >99.5% PM particles from car exhaust at high temperature.

**KEYWORDS:** Air filtration, PM<sub>2.5</sub> filter, nanofiber, high temperature, polyimide



Air pollution has become a major environmental concern due to the large amount of air pollutants emitted from human activities such as traffic, industry, and power plants. One of the major air pollutants is particulate matter (PM), particularly in many developing countries.<sup>1</sup> Figure 1, panel a shows a map of average concentration of PM<sub>2.5</sub> (defined as PM with aerodynamic diameter less than 2.5 μm) in eastern China (with the highest population) from April to August in 2014,<sup>2</sup> which indicates that the average PM<sub>2.5</sub> pollution is significant over large areas of eastern China. More than 90% of China's population experienced unhealthy PM<sub>2.5</sub> for at least 120 h during the above period, and 46% of China's population experienced PM<sub>2.5</sub> above the highest US environmental protection agency (EPA) threshold ("hazardous", > 250 μg/m<sup>3</sup>).<sup>2</sup> PM is a complex mixture of small particles and liquid droplets composed of various chemical components including inorganic matter (e.g., silicates, sulfates, and nitrates) and organic matter (e.g., organic carbon and elemental carbon, etc.).<sup>3–5</sup> PM seriously affects the living environments in terms of air quality, visibility, radiative forcing, climate effects, and ecosystems.<sup>6–11</sup> Particularly, PM<sub>2.5</sub> poses serious threat to human health since it carries a lot of toxic compounds and can penetrate the human bronchi and lungs due to its small size. Numerous epidemiological studies have demonstrated that long-term exposure to PM<sub>2.5</sub> can result in various respiratory and cardiovascular diseases and even lung cancer, increasing morbidity and mortality.<sup>12–20</sup> Besides, compared with PM<sub>10</sub> (defined as PM with aerodynamic diameter less than 10 μm), which has a short lifetime in air from minutes to hours and a limited traveling distance, the lifetime of PM<sub>2.5</sub> in air can be days to weeks, and it can cause a regional and even global effect.

Nevertheless, the control and removal of PM, especially PM<sub>2.5</sub>, remains a great challenge because of its small size, complex composition, sources, and evolution processes.<sup>21</sup>

Two types of air filters have been in common use.<sup>22</sup> One is a porous membrane filter based on size exclusion filtration. The other type is thick fibrous air filter of diverse diameters from several microns to tens of microns. However, both types of filters have significant air pressure drop, and the removal efficiency of PM<sub>2.5</sub> is limited. Recently, our group developed a transparent nanofiber air filter for the high efficiency PM<sub>2.5</sub> removal,<sup>23</sup> which can be used for personal and building protection. Different from the existing filters based on nonpolar polymers, we found that the polar chemical functional groups (i.e., in polyacrylonitrile (PAN) polymer) are important to have strong binding affinity with PM<sub>2.5</sub>. Some other recent developments on using carbon nanotubes<sup>24</sup> and polymer nanofibers<sup>25</sup> are notable examples toward PM<sub>2.5</sub> filtration. However, to eliminate the emission of PM into the air, the ultimate solution would be to remove PM from the sources often with high temperature. This calls for a new technology capable of high temperature air filtration.

It is important to identify the PM sources and evolution processes for the effective control and removal of PM pollution. Many studies have been conducted to characterize the composition and evolution processes of PM, particularly PM<sub>2.5</sub>.<sup>2–4,6,19,26–30</sup> As for the sources of PM<sub>2.5</sub>, here we take

**Received:** February 22, 2016

**Revised:** May 6, 2016

**Published:** May 11, 2016

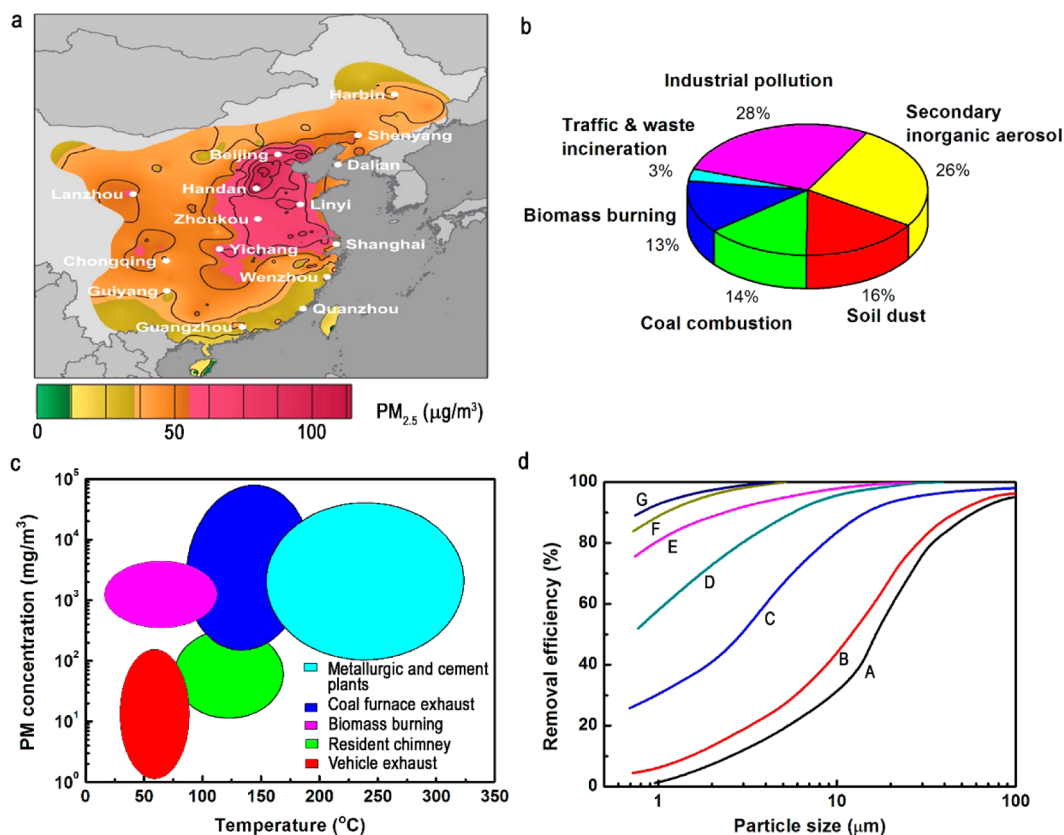


**Figure 1.** Sources and temperature distribution of PM and the PM removal performance of different industrial dust collectors. (a) Map of average concentration of  $PM_{2.5}$  in eastern China from April to August in 2014.<sup>2</sup> (b) Sources of  $PM_{2.5}$  in Beijing.<sup>4</sup> (c) Temperature and PM concentration distribution of various high temperature PM sources. (d) Comparison of PM removal performance of different industrial dust collectors.<sup>35</sup> A, baffled settling chamber; B, cyclone “off the shelf”; C, carefully designed cyclone; D, electrostatic precipitator; E, spray tower; F, Venturi scrubber; G, bag filter.

Beijing, the capital of China, as an example. Six main primary sources of  $PM_{2.5}$  in Beijing shown in Figure 1, panel b are industrial pollution, secondary inorganic aerosol, soil dust, coal combustion, biomass burning, and traffic and waste incineration emission.<sup>4</sup> Secondary inorganic aerosols are formed through the nanocondensation and growth of gaseous  $SO_x$ ,  $NO_x$ ,  $NH_3$ , and volatile organic compounds (VOCs), which are more deadly on a mass per unit volume basis.<sup>20</sup> Each of these sources has an annual mean contribution of 28, 26, 16, 14, 13, and 3% to  $PM_{2.5}$ , respectively. Among the above sources,  $PM_{2.5}$  from industrial pollution, coal combustion, biomass burning, and traffic and waste incineration is usually of high temperature, and it contributes to more than 58% of the total  $PM_{2.5}$  emissions. Not only in Beijing, but also in many other places, most of the  $PM_{2.5}$  are from high temperature sources such as industrial exhaust, coal combustion, vehicle exhaust, biomass burning, etc.<sup>12,17,21,26–28</sup> Figure 1, panel c shows the concentration and temperature distribution of PM particles from high-temperature sources.<sup>29–31</sup> Most of the PM sources contain a large amount of PM particles of various sizes with temperature of 50–300  $^{\circ}C$ . Therefore, the direct removal of PM from the sources at high temperature is a key issue to address for the effective control and abatement of PM pollution.

High temperature dust removal from exhaust gas has recently attracted more attention.<sup>29–34</sup> However, existing technology could not meet the requirement of high-efficiency  $PM_{2.5}$  removal at high temperature. As shown in Figure 1, panel d, most of the industrial dust collectors, such as cyclones,

scrubbers, and sedimentation tanks, are only effective for removing particles larger than 10  $\mu m$ , but they are ineffective for particles smaller than 10  $\mu m$ .<sup>35</sup> The cyclones, spray towers, and Venturi scrubbers consume a lot of energy and have large flow resistance (i.e., the pressure drop is high) during operation. The electrostatic precipitators have high construction and operation cost, and their PM removal efficiency depends on the PM properties such as sizes, charge states, and conductivity and drops significantly for  $PM_{2.5}$ . Although micron-sized fibrous filters are relatively effective for small particles, most of the fibrous filters cannot work at high temperature (usually  $<100^{\circ}C$ ) and have large pressure drop.

It is of great significance to develop high-efficiency filters with low flow resistance for the  $PM_{2.5}$  removal at high temperature. Here, we demonstrate a novel high-temperature polyimide (PI) nanofiber air filter, which has attractive attributes of high thermal stability (stable up to 370  $^{\circ}C$ ), high  $PM_{2.5}$  removal efficiency, low resistance to air flow, lightweight, and long working lifetime.

We chose PI as the high temperature air filter material because of its excellent thermal stability at high temperatures. PI is a polymer of imide monomers and is known for thermal stability and good chemical resistance as well as excellent mechanical properties. However, it is not yet known about their capability to remove PM in the air at high temperature. On the basis of our previous study,<sup>23</sup> polar functional groups are important to bind with PM, and we believe that PI has the right polar group for this purpose. There are various types of PIs in

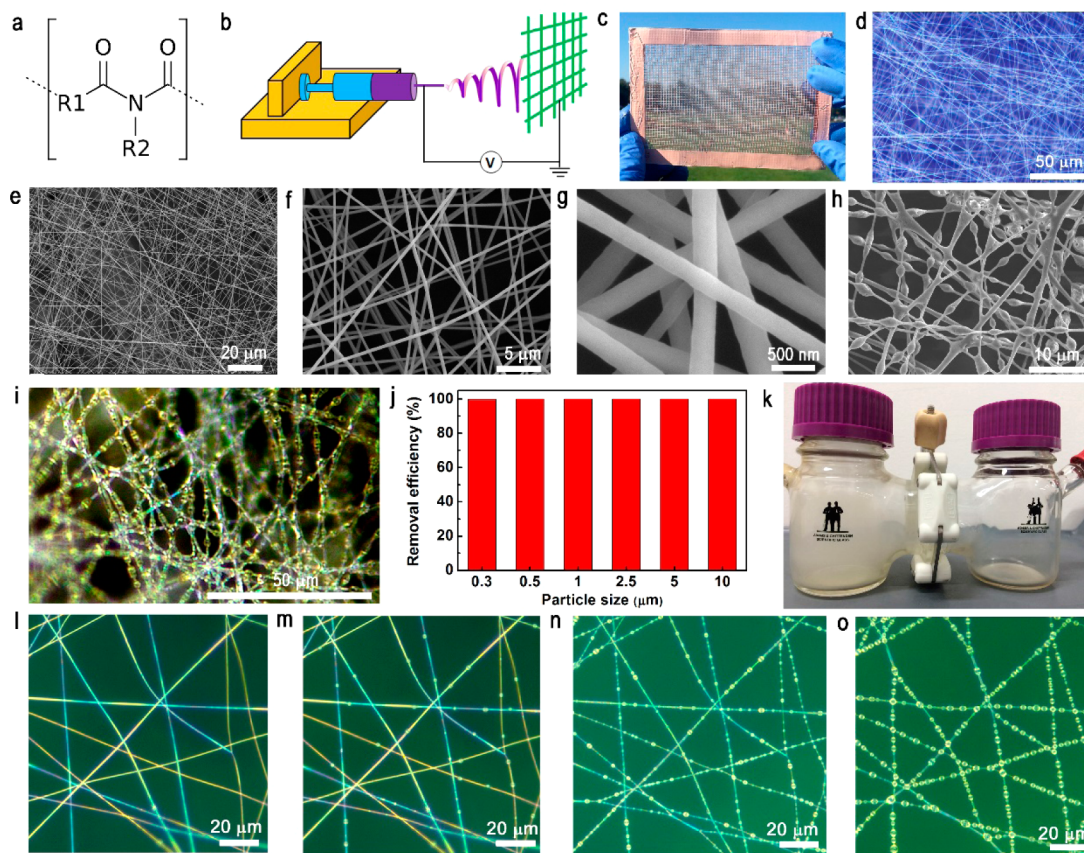


**Figure 2.** Structure and PM removal performance of PI nanofiber air filters at room temperature. (a) General molecular structure of PI. (b) Schematics of fabricating transparent PI air filters by electrospinning. (c) Photograph of a typical transparent PI air filter with optical transmittance of 70%. (d) OM image of a transparent PI air filter. (e–g) SEM images of PI air filters with different magnification. (h) SEM image of a PI air filter with captured PM particles. (i) OM image of a PI air filter with captured PM particles. (j) PM removal efficiency of PI air filters with optical transmittance of 50%. (k) Demonstration of using PI nanofiber air filter to block the PM from the sources (left bottle) entering the environment (right bottle). (l–o) In situ evolution study of PM capture by PI air filter under OM at different time sequences during a continuous feed of PM gas. The time scales for panels l–o are 0, 5, 60, and 150 s, respectively.

terms of molecular structures. A general molecular structure of PI is shown in Figure 2, panel a. For this type of PI molecule, the large dipole moment, 6.16 D, is favorable for PM filtration. We fabricated PI nanofiber air filters using electrospinning of PI–dimethylformamide solution. Electrospinning is a versatile processing technique of preparing uniform nanofiber filters from diverse polymer solutions with controllable dimensions (Figure 2b).<sup>36</sup> For the synthesis of uniform PI nanofibers, the key is to search for a suitable solution concentration and a suitable distance and voltage between the syringe tip and the grounded fiber collector. The collectors used here were copper meshes. By changing the solution concentration and the applied voltage, the diameter of PI nanofibers can be tuned accordingly. At a given working voltage and distance between the syringe tip and the collector, the optical transparency and thickness of PI nanofiber air filters primarily depend on the electrospinning time. Figure 2, panel c shows a photo of typical transparent PI air filter fabricated by electrospinning. As shown by the optical microscope (OM) and scanning electron microscope (SEM) images in Figure 2, panels d–f, the as-made PI nanofibers were uniformly distributed on the mesh substrates. The holes are much larger than the fiber diameters, allowing the substantial air flow with little resistance. Our previous study found that the fiber dimensions significantly affect the PM removal efficiency.<sup>23</sup> The fibers with small

diameters have a much higher available specific surface area than those with large diameters. The diameter of PI nanofibers fabricated here was chosen to be  $\sim 300$  nm (Figure 2g).

The PM particles used in this study were generated by burning incenses, which is a good model system for the air filtration as it contains a wide range of PM particles with various sizes and many of the components present in polluted air during hazy days, such as CO, CO<sub>2</sub>, NO<sub>2</sub>, and SO<sub>2</sub>, and also VOCs such as benzene, toluene, xylenes, aldehydes, polycyclic aromatic hydrocarbons, and other contaminants.<sup>37</sup> We used a measurement protocol previously developed in our group (see Methods).<sup>23</sup> As shown in Figure 2, panels h and i, the PI nanofibers were coated with many PM particles after filtration. The particles formed a coating layer strongly attached to the surface of nanofibers. Figure 2, panel j shows the PM removal efficiency of a PI filter with optical transmittance of 50% (the thickness is about 30–60 μm) at room temperature. Here we use the optical transmittance to indicate the thickness of the filters, which correlates with the air flow resistance. It has very high PM removal efficiency for particles with different sizes. For example, despite the small thickness of our filters, the PM removal efficiency for particles with sizes of 0.3 μm is as high as 99.98%, which reaches the standard of high-efficiency particulate air (HEPA) filters defined as filters with filtration efficiency >99.97% for 0.3 μm airborne particles. Figure 2, panel

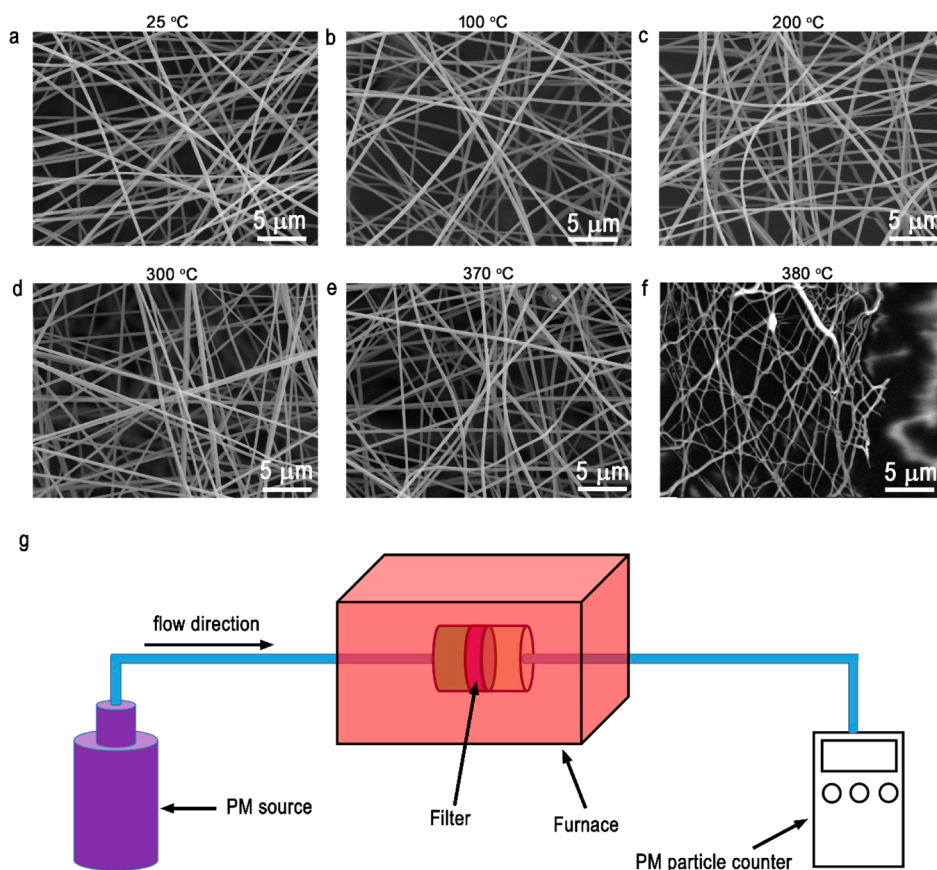


**Figure 3.** Thermal stability of PI air filters and setup of high temperature PM removal efficiency measurement. (a–f) Structure and morphology comparison of PI air filters at different temperatures. (g) Schematic illustration of the setup for high temperature PM removal efficiency measurement.

k shows a demonstration of using PI air filter to block high-concentration PM pollution. The left bottle contained a hazardous level of PM with  $PM_{2.5}$  concentration higher than  $500 \mu\text{g}/\text{m}^3$ , and the PI filter with optical transmittance of 65% was placed between the two bottles. The PI filters successfully blocked the PM from moving to the right bottle. Even after approximately 1 h, the right bottle was still very clear, and the  $PM_{2.5}$  concentration remained at a low level ( $<20 \mu\text{g}/\text{m}^3$ , less than 4% of the left side bottle).

We also studied the PM capture process and mechanism of the PI nanofibers by in situ OM imaging. As shown in Figure 2, panels l–o, with the continuous flow of high concentration smoke PM to PI filters, PM particles were captured by the PI nanofibers and attached tightly on them. With the continuous feeding of smoke PM, more PM particles were attached. Meanwhile, small particles gradually merged into larger ones. As shown by Figure 2, panel h, compared with the single PI nanofibers, more PM particles merged together around the junctions of the nanofibers and formed even larger ones.

**High Temperature PM Removal Performance of PI Nanofiber Air Filters.** The thermal stability of air filters is a key factor affecting their filtration performance at high temperature. Before testing the high-temperature performance of PI nanofiber air filters, we first checked their thermal stability. The PI nanofibers were placed in a box furnace set with different temperature in air. Each sample was kept for 1 h at each temperature. As shown by Figure 3, panels a–e, when the temperature increased from 25 to 370 °C, both the diameter and the morphology of the PI nanofibers were kept

unchanged, which show their high thermal stability. Only when the temperature increased to 380 °C did the structure of PI nanofibers began to break down. A big hole appeared in the PI nanofiber filters (Figure 3f). The PI nanofibers had evident deformation and most of them distorted. The diameter of PI nanofibers became smaller, and some of them even fractured. As shown in Figure 1, panel c, the temperature of most exhaust gases is lower than 300 °C, so the PI nanofibers would be expected to be stable when used for removing PM particles from these exhaust gases.

To test the PM removal performance of the as-made PI air filters at high temperature, we designed a testing device as shown in Figure 3, panel g. A PI filter was placed inside a furnace and connected with the filtration performance testing system. A PM particle counter was used to measure the particle number concentration. The PM used in this study was generated by burning incenses and the particle concentration of each size kept relatively stable during the testing period (see Supplementary Figure S1). The removal efficiencies were calculated by comparing the PM particle concentration with and without PI filters.

We systematically studied the PM removal efficiency of PI filters with different optical transparency at different temperatures. As shown in Figure 4, panels a (for  $PM_{2.5}$  removal) and b (for  $PM_{2.5-10}$  removal), for filters with a wide range of optical transmittance, the PI nanofiber filters show excellent thermal stability, and their filtration performance kept almost unchanged at temperature below 350 °C. For PI filters with optical transmittance of about 60%, the  $PM_{2.5}$  removal

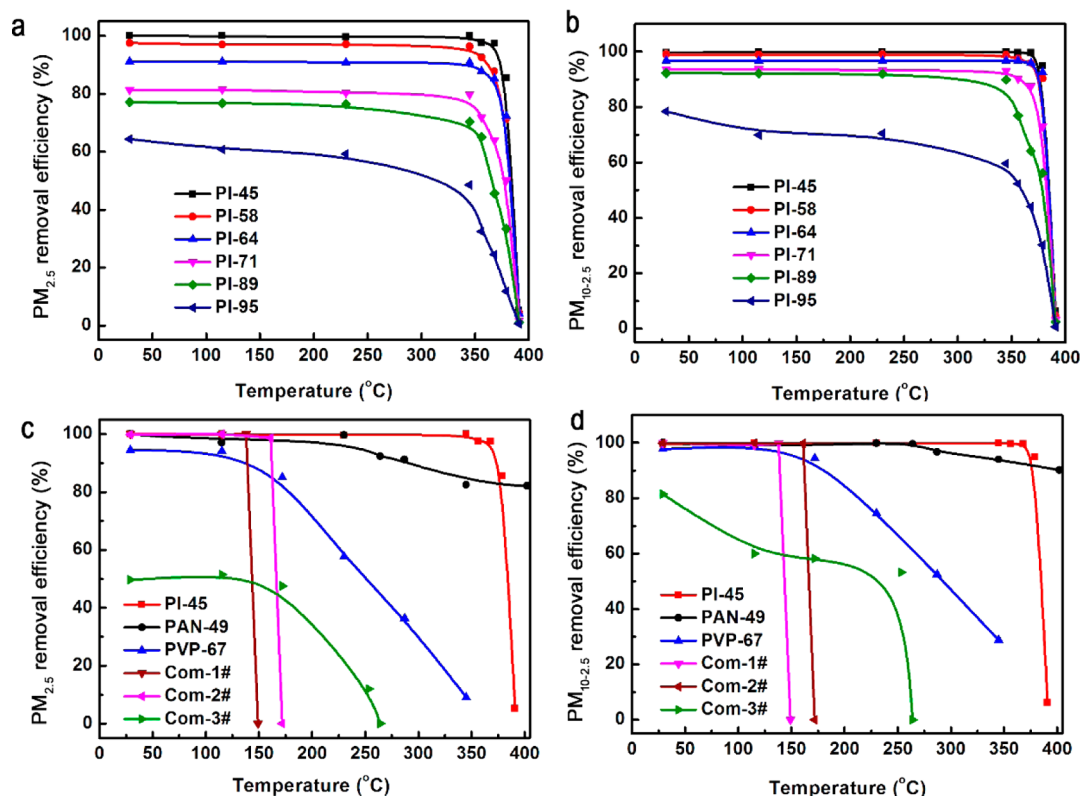


**Figure 4.** Comparison of PM removal efficiency of different air filters. (a) Comparison of PM<sub>2.5</sub> removal efficiency of PI nanofiber air filters with different transparency at the flow rate of 0.2 m/s. Here, PI-45 means PI nanofiber air filter with optical transmittance of 45%, and others have similar meanings. (b) Comparison of PM<sub>2.5-10</sub> removal efficiency of PI air filters with different optical transmittance. (c) Comparison of PM<sub>2.5</sub> removal efficiency of different air filters made of different materials. Here, “Com-” means commercial air filter. (d) Comparison of PM<sub>2.5-10</sub> removal efficiency of different air filters made of different materials.

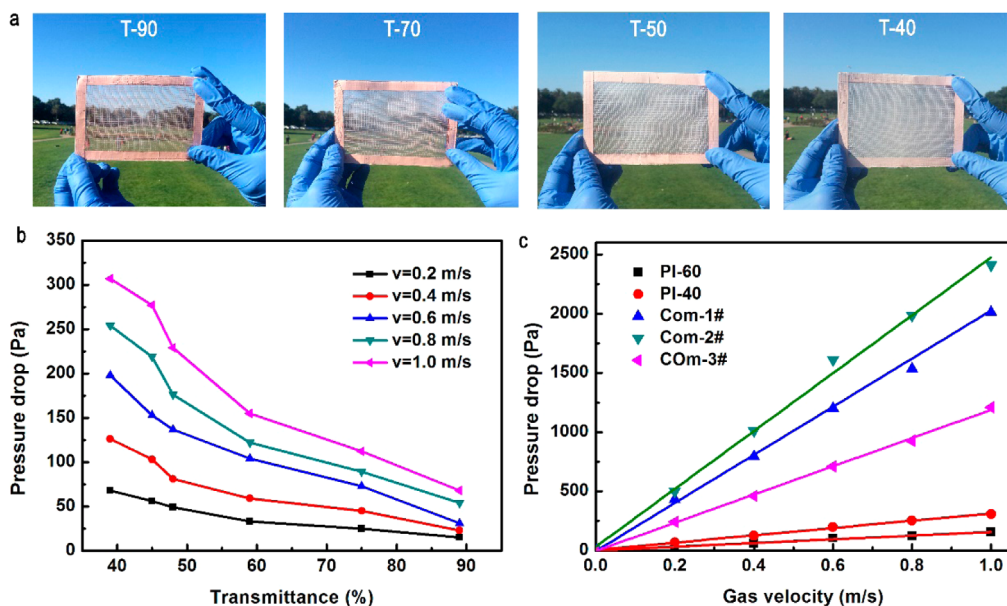


**Figure 5.** Comparison of transparency and pressure drop of transparent PI air filters with different transmittance. (a) Photographs of PI transparent air filters with different transmittance. (b) Relationship of pressure drop and transmittance at different flow rate for PI filters. (c) Comparison of pressure drop of different air filters.

efficiency was higher than 95%, which reached the standard of high-efficiency filters. For PI filters with optical transmittance of about 45%, the PM<sub>2.5</sub> removal efficiency was higher than 99.98%, which reached the standard of HEPA filters defined as

filters with filtration efficiency >99.97% for 0.3 μm airborne particles. With the temperature increase, they were stable and their filtration performance kept unchanged. Only when the temperature was higher than 350 °C did the structure of PI

filters begin to change and the PM removal efficiency begin to decrease. When the temperature reached 390 °C, the PI filters were seriously damaged, and the PM removal efficiency almost became zero.

To obtain a better comparison, we also tested air filters made of other polymers such as polyacrylonitrile (PAN), polyvinylpyrrolidone (PVP), and three kinds of commercial air filters. The PAN and PVP also had diameters of about 300 nm. As shown by Figure 4, panels c and d, it is evident that among the six different kinds of air filters, the PI filters exhibited the best filtration performance at high temperature. The dipole moment for PI, PAN, and PVP is 6.2, 3.6, and 2.3 D, respectively,<sup>23</sup> indicating the stronger adhesion of PM on PI nanofibers. For PI filters with optical transmittance lower than 90%, both the PM<sub>2.5-10</sub> and PM<sub>2.5</sub> removal efficiency kept almost unchanged at the temperature range of 25–350 °C. Compared with PI, the PAN filters also have high PM removal efficiency at room temperature as shown in our previous study.<sup>23</sup> However, when the temperature increased to 230 °C, the PM removal efficiency of PAN filters gradually decreased. PAN is thermally oxidized in air to form an oxidized PAN fiber when temperature is higher than 230 °C (Figure S2). The surface chemistry of PAN has a large change after oxidation, which is likely to directly influence the adhesion of PM on the PAN nanofibers. As for the PVP filters, their filtration performance has an obvious decrease when the temperature is higher than 150 °C. For the three kinds of commercial filters, their thermal stability is even worse. For example, when the temperature is higher than 150 °C, the commercial 1# (i.e., Com-1#) filter completely melts. The Com-2# filter has a similar phenomenon when the temperature increases to 170 °C. The Com-3# filter has a poor filtration performance even at room temperature. When the temperature increased to 200 °C, the Com-3# filter gradually melts. From the above comparison, the PI nanofiber filters have the best PM removal performance and the best thermal stability.

In addition to the PM removal efficiency, another important desirable parameter is the air flux with low pressure drop. It was reported that energy consumption is directly proportional to the pressure drop over the filters and normally accounts for 70% of the total life cycle cost of air filters.<sup>38</sup> In the average commercial building, 50% of the energy bill is for the HVAC (heating, ventilation, and air conditioning) system, and 30% of that is directly related to the air filtration.

There is usually a trade-off between two important filtration parameters: high removal efficiency and low pressure drop at high flow rates. The overall performance of the air filters considering both efficiency and pressure drop may be defined by a quality factor (QF),  $QF = -\ln(1 - E)/\Delta P$ , where  $E$  is PM removal efficiency and  $\Delta P$  is the pressure drop of the filters. The higher the QF, the better the filter. As shown in Figure 5, panel a, there are four PI nanofiber air filters with different optical transmittance. Here, we compare the pressure drop of PI nanofiber filters with different optical transmittance under a variety of air flow rate (Figure 5b). Figure S3 shows a schematic of the pressure drop measurement. As shown in Figure 5, panel b, with the decrease of optical transmittance, the pressure drop of PI air filters increases. However, even for the thickest PI filters with the lowest optical transmittance at 40%, the pressure drop is only ~70 Pa at a gas velocity of 0.2 m/s. Even at a gas velocity of 1 m/s, the pressure drop for PI filters with optical transmittance of 40% is only about ~300 Pa. In comparison, the three different commercial air filters have much higher pressure drop than PI air filters (Figure 5c). Although Com-1#

and Com-2# commercial air filters have high PM removal efficiency (Figure 4c and d), their pressure drop is too large to allow for a high air flow (Figure 5c). For example, at the flow rate of 0.6 m/s, PI-40 (40% optical transmittance) with similarly high PM removal efficiency has a small pressure drop of ~200 Pa, while Com-1# and Com-2# have a pressure drop about an order of magnitude higher at 1200 and ~1600 Pa, respectively. An overall performance comparison of different air filters at the flow rate of 0.2 m/s is summarized in Table 1,

**Table 1. Performance Summary of Different Air Filters<sup>a</sup>**

sample	$T$ (%)	$E$ (%)	$\Delta P$ (Pa)	QF (Pa <sup>-1</sup> )	$t$ (°C)
PI-40	40	99.97	73	0.1072	370
PI-60	60	97.02	45	0.078	370
PAN-45	49	99.97	80	0.1014	230
PVP-67	67	94.43	71	0.0407	150
Com-1#	7.3	99.91	433	0.0162	140
Com-2#	6.5	99.87	499	0.0133	160
Com-3#	13	49.66	243	0.0028	170

<sup>a</sup>Note:  $T$ , optical transmittance;  $E$ , PM<sub>2.5</sub> removal efficiency;  $\Delta P$ , pressure drop at the flow rate of 0.2 m/s; QF, quality factor;  $t$ , highest stable-working temperature.  $QF = -\ln(1 - E)/\Delta P$ .

which clearly shows that PI nanofiber filters have the best air filtration performance considering PM removal efficiency, pressure drop, the quality factor, and the highest stable-working temperature.

The reason for the PI nanofiber air filters having such low pressure drop lies in the following two aspects. First, the nanofiber diameter is small, and the PI nanofiber air filters have a small thickness. The thickness of PI nanofiber filters is in the range of 0.01–0.1 mm compared to traditional fiber filters with thickness of 2–30 mm. There is a lot of empty space between nanofibers. Second, when the diameter of the nanofibers is comparable to the mean free path of the air molecules (66 nm under normal conditions), the gas velocity is nonzero at the fiber surface due to “slip” effect. Because of the “slip” effect, the drag force from the nanofibers onto the air flow is greatly reduced, thus greatly reducing the pressure drop.

The long-term and field-test performance is very important for the practical application of PI nanofiber air filters in real environments. The long-term performance of the PI nanofiber air filters was evaluated by using a PI filter with optical transmittance of 55% under the condition of hazardous level equivalent to the PM<sub>2.5</sub> index >300 and mild wind condition (the wind speed is about 0.2 m/s). The long-term PM particle removal performance of PI filters is shown in Figure 6, panel a. After continuously working for 120 h, the PI air filter still maintained a high PM removal efficiency. As shown in Figure 6, panel a, the PM<sub>2.5</sub> and PM<sub>2.5-10</sub> removal efficiency is kept as high as 97–99% and 99–100%, respectively, while the pressure drop only increased less than 10 Pa. They can even work for nearly 300 h (Figure S4). We also tested the particle removal efficiency of the PI filters in practical environments. As shown in Figure 6, panels b and c, we used a PI filter with optical transmittance of 50% to remove the PM particles from the car exhaust gas. The temperature of the car exhaust usually ranges from 50–80 °C. A PM particle counter was used to measure the PM concentration in the exhaust gas before and after filtration. The PI filter was kept stable under the strong blowing by the exhaust with a gas velocity of 2–3 m/s. The PM concentrations in the exhaust before and after filtration were

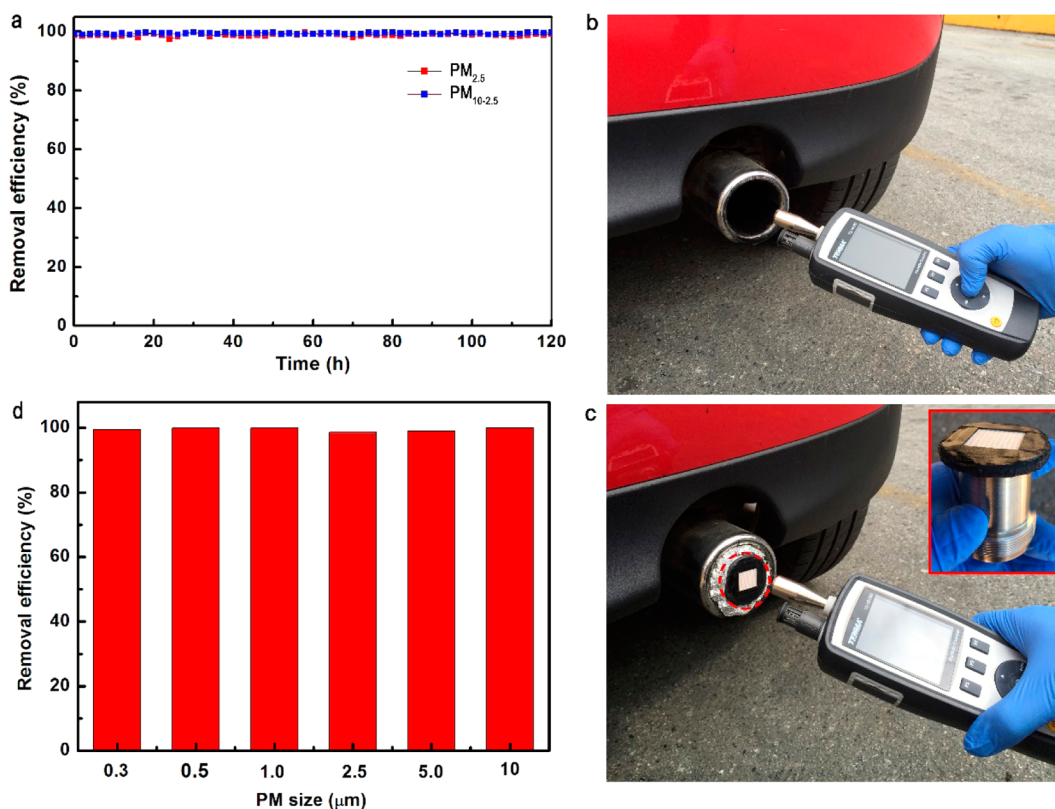


**Figure 6.** Long-term and field-test performance of PI air filters. (a) The long-term  $PM_{2.5}$  and  $PM_{2.5-10}$  removal efficiency by PI nanofiber air filters with transmittance of 50% under continuous hazardous level of PM pollution. (b) PM number concentration measurement of car exhaust without air filter. (c) PM number concentration measurement of car exhaust with air filter. The inset shows a stainless steel pipe coated with a PI filter with transmittance of 50% shown by the red circle in panel c. (d) Removal efficiency of PM particles from car exhaust gas.

shown in Figure 6, panel d, from which we can see that the PI filter can effectively remove all kinds of particles with sizes from  $<0.3 \mu\text{m}$  to  $>10 \mu\text{m}$  with very high efficiency. Especially, after filtration, the PM concentration of the exhaust was decreased to almost the same with that of clean ambient air, clearly showing the high filtration efficiency of PI nanofiber filters at both room and high temperature.

In summary, we have shown that the PI nanofiber filters have high filtration efficiency, low pressure drop, and excellent temperature stability compared to common commercial air filters. The high efficiency results from the polar chemical functional groups in PI molecules in conjunction with static charge deposited into nanofiber during electrospinning, which can attract and bind strongly with  $PM_{2.5}$ . The temperature stability comes from the intrinsic molecular structure of PI polymer. The PI filters also allow a high air flux with very low pressure drop. The long-term performance test shows that the PI air filters have a high PM particle removal efficiency and a long lifetime. The PI filters can effectively remove almost all the PM particles from the car exhaust at high temperature. The above performance proves that the PI nanofiber air filters can be used as very effective high-efficiency air filters for high temperature  $PM_{2.5}$  particles removal. For the industrial application of PI air filters, they can work both independently and work together with the industrial dust collectors at both room and high temperature.

**Methods.** *Electrospinning.* The solution system for the polymers used in this study was 15 wt % PI resin (CAS #62929-02-6, Alfa Aesar) in dimethylformamide (EMD Millipore), 10 wt % PAN (MW =  $1.5 \times 10^5$  g/mol, Sigma-

Aldrich) in dimethylformamide (EMD Millipore), and 8 wt % polyvinylpyrrolidone (MW =  $1.3 \times 10^6$  g/mol, Across) in ethanol (Fisher Scientific). A 1 mL syringe with a 22-gauge needle tip was used to load the polymer solution and connected to a voltage supply (ES30P-5W, Gamma High Voltage Research). A syringe pump (KD Scientific) was used to pump the solution out of the needle tip. The electrospun nanofibers were collected by a grounded copper mesh. The wire diameter of the copper mesh was 0.011 in., and the mesh size was  $18 \times 16$ . During electrospinning, the nanofibers would lie across the mesh hole to form the air filter.

*PM Generation and Efficiency Measurement.* The PM particles used in this work were generated by burning incense. The incense smoke PM particles had a wide size distribution from  $<300 \text{ nm}$  to  $>10 \mu\text{m}$ , with the majority of particles being  $<1 \mu\text{m}$ . By diluting the smoke PM by air, the inflow concentration was controlled to a hazardous pollution level equivalent to the  $PM_{2.5}$  index  $>300$ . A particle counter (CEM) was used to detect the PM particle number concentration before and after filtration. The removal efficiency was calculated by comparing the number concentration before and after filtration.

*High Temperature Filtration Measurement.* The high temperature filtration measurement was conducted on an electrical tube furnace (Lindberg/Blue). First, a PI filter was coated by copper tape on the edge. Then the filter was placed between two stainless steel pipe flanges and fixed firmly with screws. Then the pipe flanges were connected into the filtration measurement system and placed inside the tube furnace. A PM particle counter (CEM) was used to measure the particle

number concentration. For each temperature, the filter was kept for 20 min to be stabilized.

**Optical Transmittance Measurement.** The optical transmittance measurement was conducted as follows. A xenon lamp (69911, Newport) was used as the light source, coupled with a monochromator (74125, Newport) to control the wavelength. The beam size was trimmed by an iris to  $\sim 5 \text{ mm} \times 5 \text{ mm}$  before it entered an integrating sphere (Newport) for transmittance measurement. A photodiode was connected to lock-in radiometry system (70100 Merlin, Newport) for photocurrent measurement. A photodetector (70356, Newport) was inserted into one of the ports of integrating sphere. The filter samples were placed in front of the integrating sphere. Both specular transmittance and diffuse transmittance were included. For air filters collected on copper mesh, a clean copper mesh with the same geometry was used as a reference. For self-standing filters, ambient air was used for reference. The transmittance spectrum was weighted by AM1.5 solar spectrum from 400–800 nm to obtain the average transmittance.

**Pressure Drop Measurement.** The pressure drop was measured by a differential pressure gauge (EM201B, UEi test instrument).

**Characterization.** The SEM images were taken by FEI XL30 Sirion SEM with an acceleration voltage of 5 kV for imaging.

## ■ ASSOCIATED CONTENT

### Supporting Information

The Supporting Information is available free of charge on the ACS Publications website at DOI: [10.1021/acs.nanolett.6b00771](https://doi.org/10.1021/acs.nanolett.6b00771).

Size distribution of PM particles generated by incense burning over time; comparison of structure and morphology of different air filters at different temperature; schematic of pressure drop measurement (PDF)

## ■ AUTHOR INFORMATION

### Corresponding Author

\*E-mail: [yicui@stanford.edu](mailto:yicui@stanford.edu).

### Author Contributions

R.Z., C.L., P.-C.H., S.C., and Y.C. conceived the concept, and Y.C. and S.C. supervised the project. R.Z., C.L., and P.-C.H. designed the experiments, fabricated the filters, and measured the filtration performance. R.Z. did the SEM characterization and long-term performance test. R.Z., P.-C.H., C.Z., N.L., and J.Z. designed and constructed the high temperature testing setup. R.Z., P.-C.H., and C.Z. measured the transparency of filter. R.Z., H.R.L., and J.Z. measured the contact angles of filters. R.Z., P.-C.H., and Y.Q. measured the pressure drop of the filters. R.Z., C.Z., and Y.L. did the field-test performance. R.Z., C.L., P.-C.H., S.C., and Y.C. analyzed the data. R.Z. and Y.C. wrote the paper. All the authors discussed the whole paper.

### Notes

The authors declare no competing financial interest.

## ■ ACKNOWLEDGMENTS

We acknowledge Yuanqing Li, Meng Ye, and Wenting Zhao for fruitful discussions.

## ■ REFERENCES

- Fang, M.; Chan, C. K.; Yao, X. *Atmos. Environ.* **2009**, *43*, 79–86.
- Rohde, R. A.; Muller, R. A. *PLoS One* **2015**, *10*, e0135749.
- Seinfeld, J. H. *Science* **1989**, *243*, 745–752.
- Zhang, R.; Jing, J.; Tao, J.; Hsu, S.-C.; Wang, G.; Cao, J.; Lee, C.; Zhu, L.; Chen, Z.; Zhao, Y.; Shen, Z. *Atmos. Chem. Phys.* **2013**, *13*, 7053–7074.
- Maricq, M. M. *J. Aerosol Sci.* **2007**, *38*, 1079–1118.
- Watson, J. G. *J. Air Waste Manage. Assoc.* **2002**, *52*, 628–713.
- Streets, D. G.; Wu, Y.; Chin, M. *Geophys. Res. Lett.* **2006**, *33*, 1–4.
- Andreae, M.; Rosenfeld, D. *Earth-Sci. Rev.* **2008**, *89*, 13–41.
- Mahowald, N. *Science* **2011**, *334*, 794–796.
- Horton, D. E.; Skinner, C. B.; Singh, D.; Diffenbaugh, N. S. *Nat. Clim. Change* **2014**, *4*, 698–703.
- Nel, A. *Science* **2005**, *308*, 804–806.
- Betha, R.; Behera, S. N.; Balasubramanian, R. *Environ. Sci. Technol.* **2014**, *48*, 4327–4335.
- Wu, S.; Deng, F.; Wei, H.; Huang, J.; Wang, X.; Hao, Y.; Zheng, C.; Qin, Y.; Lv, H.; Shima, M.; Guo, X. *Environ. Sci. Technol.* **2014**, *48*, 3438–3448.
- Brook, R. D.; Rajagopalan, S.; Pope, C. A.; Brook, J. R.; Bhatnagar, A.; Diez-Roux, A. V.; Holguin, F.; Hong, Y.; Luepker, R. V.; Mittleman, M. A.; et al. *Circulation* **2010**, *121*, 2331–2378.
- Anenberg, S. C.; Horowitz, L. W.; Tong, D. Q.; West, J. *Environ. Health Persp.* **2010**, *118*, 1189–1195.
- Timonen, K. L.; Vanninen, E.; De Hartog, J.; Ibaldo-Mulli, A.; Brunekreef, B.; Gold, D. R.; Heinrich, J.; Hoek, G.; Lanki, T.; Peters, A.; et al. *J. Exposure Sci. Environ. Epidemiol.* **2006**, *16*, 332–341.
- Zhao, S.; Chen, L.; Li, Y.; Xing, Z.; Du, K. *Atmosphere* **2015**, *6*, 234–254.
- Hoek, G.; Krishnan, R. M.; Beelen, R.; Peters, A.; Ostro, B.; Brunekreef, B.; Kaufman, J. D. *Environ. Health* **2013**, *12*, 1–15.
- Raaschou-Nielsen, O.; Andersen, A. J.; Beelen, R.; Samoli, E.; Stafoggia, M.; Weinmayr, G.; Hoffmann, B.; Fischer, P.; Nieuwenhuijsen, M. J.; Brunekreef, B.; et al. *Lancet Oncol.* **2013**, *14*, 813–822.
- Hu, D.; Jiang, J. *J. Environ. Prot.* **2013**, *04*, 746–752.
- Sun, Y.; Wang, Z.; Fu, P.; Yang, T.; Jiang, Q.; Dong, H.; Li, J.; Jia, J. *Atmos. Chem. Phys.* **2013**, *13*, 4577–4592.
- Hinds, W. C. *Aerosol Technology: Properties, Behavior, and Measurement of Airborne Particles*; Wiley-Interscience: New York, 1982; Vol. 1.
- Liu, C.; Hsu, P.-C.; Lee, H.-W.; Ye, M.; Zheng, G.; Liu, N.; Li, W.; Cui, Y. *Nat. Commun.* **2015**, *6*, 1–9.
- Li, P.; Zong, Y.; Zhang, Y.; Yang, M.; Zhang, R.; Li, S.; Wei, F. *Nanoscale* **2013**, *5*, 3367–3372.
- Gong, G.; Zhou, C.; Wu, J.; Jin, X.; Jiang, L. *ACS Nano* **2015**, *9*, 3721–3727.
- Cheng, Z.; Jiang, J.; Fajardo, O.; Wang, S.; Hao, J. *Atmos. Environ.* **2013**, *65*, 186–194.
- Huang, R.; Zhang, Y.; Bozzetti, C.; Ho, K.; Cao, J.; Han, Y.; Daellenbach, K. R.; Slowik, J. G.; Platt, S. M.; Canonaco, F.; et al. *Nature* **2014**, *514*, 218–222.
- Thorpe, A.; Harrison, R. M. *Sci. Total Environ.* **2008**, *400*, 270–282.
- Ma, L.; Verelst, H.; Baron, G. *Catal. Today* **2005**, *105*, 729–734.
- Feng, S.; Xu, S.; Liu, J.; Cao, Q.; Lu, J.; Li, X.; Wang, C. *Ind. Saf. Environ. Prot.* **2009**, *1*, 6–9.
- Zhou, X.; Sui, X.; Huang, X. *Develop. Appl. Mater.* **2008**, *6*, 99–102.
- Ergüdenler, A.; Tang, W.; Brereton, C. M.; Lim, C. J.; Grace, J. R.; Gennrich, T. J. *Sep. Purif. Technol.* **1997**, *11*, 1–16.
- Heidenreich, S.; Haag, W.; Salinger, M. *Fuel* **2013**, *108*, 19–23.
- Peukert, W. *Filtr. Sep.* **1998**, *35*, 461–464.
- Peirce, J. J.; Vesilind, P. A.; Weiner, R. *Environmental Pollution and Control*; Butterworth-Heinemann: Waltham, 1998.
- Thavasi, V.; Singh, G.; Ramakrishna, S. *Energy Environ. Sci.* **2008**, *1*, 205–221.
- Lin, T.; Krishnaswamy, G.; Chi, D. S. *Clin. Mol. Allergy* **2008**, *6*, 1–9.
- Li, P.; Wang, C.; Zhang, Y.; Wei, F. *Small* **2014**, *10*, 4543–4561.